

# Proliferation of oxygen oases in Mesoarchean oceans

Hui Ye<sup>1,2</sup>, Chang-Zhi Wu<sup>1,3,\*</sup>, Xiao-Lei Wang<sup>2</sup>, Tao Yang<sup>2</sup>, Yue Guan<sup>2</sup>, Xiuqing Yang<sup>1</sup>, Weiduo Hao<sup>4</sup>, Kurt O. Konhauser<sup>5</sup>, and Weiqiang Li<sup>2,\*</sup>

<sup>1</sup>Laboratory of Mineralization and Dynamics, School of Earth Science and Resources, Chang'an University, Xi'an 710054, China

<sup>2</sup>State Key Laboratory of Critical Earth Material Cycling and Mineral Deposits, School of Earth Sciences and Engineering, Nanjing University, Nanjing 210023, China

<sup>3</sup>Xinjiang Natural Resources and Ecological Environment Research Center, Urumqi 830000, China

<sup>4</sup>State Key Laboratory of Continental Dynamics, Shaanxi Key Laboratory of Early Life and Environment, Department of Geology, Northwest University, Xi'an 710069, China

<sup>5</sup>Department of Earth and Atmospheric Sciences, University of Alberta, Edmonton, Alberta T6G 2E3, Canada

## ABSTRACT

Oxygenic photosynthesis played an essential role in the accumulation of free oxygen (O<sub>2</sub>) at Earth's surface, but questions persist regarding its evolutionary timeline. Manganese (Mn)-rich sedimentary rocks from the Mesoarchean Pongola Supergroup in South Africa have been invoked among the earliest evidence for O<sub>2</sub>-dependent Mn(II) oxidation and thus photosynthetic O<sub>2</sub> production in oceans. However, as a singular suite of rocks, uncertainties persist about whether the evidence for O<sub>2</sub> in the Pongola region has global implications. Here we report on another Mesoarchean Mn-rich iron formation in South China, dating back to ca. 2.88–2.80 Ga. The Dianzihe iron formation exhibits a positive correlation between Mn enrichment (MnO up to 7.08 wt%, Fe/Mn ratio down to 5.1) and negative δ<sup>56</sup>Fe values (−0.21 to −1.33‰; average = −0.91‰). This pattern requires oxygenated seawater (i.e., O<sub>2</sub> > 10 μM) at least to the seafloor, allowing not only for the oxidation of Fe(II) and Mn(II) but also for the preservation of Fe(Mn) oxyhydroxides until post-depositional modifications. Based on our findings in China alongside the distribution of Mn-rich iron formations in South Africa, we posit that a global distribution of oxygen oases, driven by cyanobacterial O<sub>2</sub> production, already existed in the Mesoarchean.

## INTRODUCTION

The production of O<sub>2</sub> through oxygenic photosynthesis was crucial for developing complex life dependent on aerobic respiration. It is believed that oxygenic photosynthesis facilitated the Great Oxidation Event (GOE) ca. 2.4–2.2 Ga (Poulton et al., 2021), but the evolutionary timeline of cyanobacteria—the earliest oxygenic photosynthesizers—remains uncertain due to lack of irrefutable paleontological evidence. For instance, interpretations of the structure and texture of Archean cyanobacteria microfossils have been subject to controversy (Knoll, 2003), while biomarkers in Archean sedimentary rocks have been susceptible to contamination and are not entirely diagnostic of oxygenic photosynthesis (Brocks, 2011). Molecular clock analyses have

also been limited by factors such as database size, modeling approaches, and calibration methods, but appear to converge on a Paleoproterozoic–Mesoarchean timeframe for the origin of oxygenic photosynthesis (Sánchez-Baracaldo et al., 2022). Although redox-sensitive elements and their isotope signatures in the Archean sedimentary rocks have suggested the existence of “oxygen oases” before the GOE (e.g., Czaja et al., 2012; Olson et al., 2013; Planavsky et al., 2014; Kurzweil et al., 2016; Ossa Ossa et al., 2018; Ostrander et al., 2021), the proposed timeframe for the origin of oxygenic photosynthesis varies widely from ca. 3.8 to 2.4 Ga (Lyons et al., 2014; Cardona, 2017). Clearly, more precise constraints on the evolutionary timeline of oxygenic photosynthesis are necessary.

Manganese is a unique redox-variable element to track ancient O<sub>2</sub> signals. Traditionally, the oxidation of Mn(II) to Mn(III/IV) oxyhydroxides (MnOx) was argued to require O<sub>2</sub> given the high redox potential of MnOx/Mn(II) [e.g.,

1.23 V for MnO<sub>2</sub>/Mn(II)], and MnOx burial requires an oxygenated water column because of rapid reduction of MnOx coupled to the oxidation of reductants (e.g., ferrous iron, organic matter) in anoxic waters. However, recent research has identified various O<sub>2</sub>-independent pathways for Mn(II) oxidation (Daye et al., 2019; Liu et al., 2020), and Mn enrichment in sediments can also occur by coprecipitation of Mn(II) with calcite in anoxic waters (Herndon et al., 2018). Accordingly, there is a lack of consensus on whether ancient Mn-rich sedimentary rocks are proxies for early oxygenation (Robbins et al., 2023). Considering these conflicting mechanisms, fully understanding the history of Earth's oxygen levels will remain elusive until we gain a deeper insight into the environmental significance of Mn-rich Archean sedimentary rocks.

The examination of Mn-rich iron formations in the ca. 2.99–2.87 Ga Pongola Supergroup in South Africa has been cited as the earliest evidence for O<sub>2</sub>-dependent Mn(II) oxidation and photosynthetic production of O<sub>2</sub> in Earth's ancient oceans (Crowe et al., 2013; Planavsky et al., 2014; Ossa Ossa et al., 2018). However, given the absence of contemporaneous Mn-rich sedimentary rocks from other cratons, questions arise whether the evidence for O<sub>2</sub> in the Pongola region (Eickmann et al., 2018) reflects local depositional conditions or has broader global implications. To address these uncertainties, we present new elemental and Fe isotopic data from a contemporaneous Mesoarchean Mn-rich iron formation from South China.

## GEOLOGICAL BACKGROUND AND SAMPLES

The Kongling Complex, situated in the northern portion of the Yangtze Craton, South China

Chang-Zhi Wu  <https://orcid.org/0000-0002-9647-4512>

\*corresponding authors: [wucz@nju.edu.cn](mailto:wucz@nju.edu.cn), [liweiqiang@nju.edu.cn](mailto:liweiqiang@nju.edu.cn)

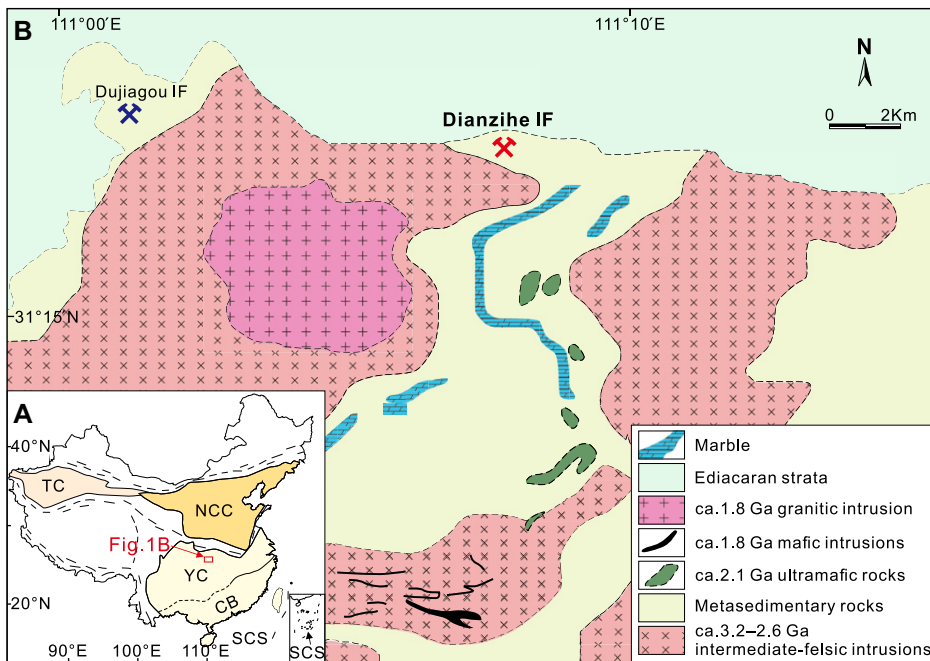


**Figure 1. (A) Schematic map of the Precambrian blocks in China. CB—Cathaysia Block; NCC—Northern China Craton; SCS—South China Sea; TC—Tarim Craton; YC—Yangtze Craton. (B) Simplified geological map of the Kongling Complex (modified from Gao et al., 1999), showing the location of the Dianzihe iron formation (IF).**

(Figs. 1A and 1B), comprises primarily intermediate-felsic intrusions and amphibolite dated to ca. 3.0–2.6 Ga, as well as overlying sedimentary rocks (Guo et al., 2015). The latter are predominantly graphite-bearing and Al-rich metapelites (Gao et al., 1999), with minor marble, quartzite, and iron formation, which were deposited on a continental shelf. These sedimentary rocks experienced multi-stage metamorphism since ca. 2.8 Ga, reaching the amphibole–granulite facies (Qiu et al., 2000; Li et al., 2014). Our samples were collected from the Dianzihe iron formation within the metasedimentary rocks of the northern Kongling Complex (Figs. 1A and 1B). This iron formation is characterized by alternating laminations (Fig. S1 in the Supplementary Material<sup>1</sup>) composed of magnetite, quartz, apatite, Fe–Mn carbonates, Fe–Mn amphiboles, Fe–Mn pyroxenoid, and garnet (Figs. S2 and S3; Tables S1 and S2), indicative of a high-grade metamorphosed iron formation (Klein, 2005). Considering the preservation of alternating laminations and the relative immobility of major elements (i.e., Fe and Mn) during post-depositional alteration, the Fe–Mn system in the iron formation was unlikely to have been significantly altered (more information on this and the analytical methods and data are presented in the Supplementary Material<sup>1</sup>).

<sup>1</sup>Supplemental Material. Methods, additional information regarding the potential metamorphic and metasomatic influences, Figures S1–S9, and Tables S1–S4. Please visit <https://doi.org/10.1130/GEOL.S.28299389> to access the supplemental material; contact [editing@geosociety.org](mailto:editing@geosociety.org) with any questions.

## RESULTS AND DISCUSSION

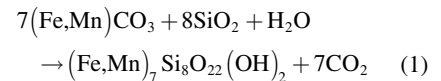
### Age of the Dianzihe Iron Formation

To determine the age of the Dianzihe iron formation, zircon grains were separated from three iron formation samples and then analyzed using secondary ion mass spectrometry. The zircon crystals of magmatic origin yielded concordant <sup>207</sup>Pb/<sup>206</sup>Pb ages of 3305–2868 Ma (Figs. S5–S7). The youngest three zircon crystals had an average <sup>207</sup>Pb/<sup>206</sup>Pb age of ca. 2.88 Ga, representing the maximum depositional age of the Dianzihe iron formation. The sedimentary rocks hosting the iron formation were magmatically altered ca. 3.0–2.6 Ga (Guo et al., 2015) and metamorphosed ca. 2.8–2.75 Ga (Qiu et al., 2000; Li et al., 2014). The absence of zircon grains in the Dianzihe iron formation that are younger than 2.88 Ga suggests that the iron formation was deposited between ca. 2.88 and 2.80 Ga. This age model is consistent with geochronological constraints on the contemporaneous Dujiagou iron formation located in the northern Kongling Complex (Zhou et al., 2022) (Fig. 1).

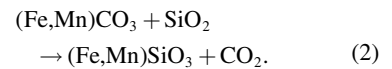
### Manganese Oxidation and O<sub>2</sub> in the Mesoproterozoic Oceans

The Dianzihe iron formation samples are characterized by elevated MnO levels, reaching up to 7.08 wt%, with an average of 3.25 wt% (Table S4). The Mn-rich minerals predominantly consist of carbonates, amphiboles, and pyroxenoids (Fig. S3). Relict Mn-rich carbonates are found within euhedral–subhedral Fe–Mn amphiboles and coexist with pyroxenoids (Fig. S2; Tables S1 and S2), implying that during meta-

morphism, Mn-rich carbonates transformed into Mn-rich amphiboles and pyroxenoids through decarbonation reactions:



and



Accordingly, initial Mn enrichment in the Dianzihe iron formation was derived from Mn-rich carbonates, which may have formed via (i) conversion of MnOx to Mn-rich carbonates during diagenesis (Planavsky et al., 2014; Ossa Ossa et al., 2018), or (ii) primary coprecipitation of Mn(II) with calcite. The latter mechanism formed Ca–Mn carbonates relying on the existence of calcite to act as nucleation sites and/or dissolution of calcite to contribute bicarbonate (Herndon et al., 2018; Wittkop et al., 2020). However, the Mn-bearing carbonates in the Dianzihe iron formation are low-CaO (average 3.3 wt%) Fe–Mn carbonates (average MnO = 33.4 wt%, average FeO = 22.6 wt%) (Table S1), indicating that these Mn-rich carbonates were likely formed via diagenesis rather than coprecipitation of Mn(II) with calcite. Importantly, this implies that the original Mn-rich mineral was MnOx.

Mn(II) oxidation has multiple pathways, including anoxygenic photosynthesis, photochemistry, and Mn(II) oxidation by O<sub>2</sub>. In the case of anoxygenic photosynthesis, there are two possible mechanisms. The first, as originally proposed by Johnson et al. (2013), has Mn(II) donating electrons directly to an ancestral reaction center in a manner akin to photoferrotochemistry, but forming MnOx instead of Fe(OH)<sub>3</sub>. This reaction is theoretically plausible, but to date no modern species using this metabolism have been identified. The second relies on H<sub>2</sub>S as the electron donor in co-cultures involving a currently unknown mechanism (Daye et al., 2019). However, sulfide availability conflicts with the Fe(II)-rich environment required for iron formation deposition (Konhauser et al., 2017). Likewise, although O<sub>2</sub>-independent photochemical oxidation of Mn(II) or rhodochrosite (MnCO<sub>3</sub>) is feasible under controlled laboratory conditions, it is limited by multiple factors, including interference from other elements, e.g., Fe(II), and limited rhodochrosite supply in the photic zone (Lyons et al., 2020).

Irrespective of the oxidation mechanism, preservation of MnOx is unlikely in anoxic waters due to its rapid reduction (e.g., on the order of days) coupled to the oxidation of reductants [e.g., Fe(II)], which is consistent with a shallow depth (e.g., <2–10 m) of MnOx pen-

etration into anoxic waters (Robbins et al., 2023). Previous studies have demonstrated that Mn-oxides begin to dissolve when  $O_2 < 100 \mu M$  but can persist to become buried when bottom water  $O_2$  concentrations are lowered to  $\sim 10 \mu M$  (Johnson et al., 1992). Accordingly, MnOx in the Dianzihe iron formation were likely formed via  $O_2$ -dependent Mn(II) oxidation in oxic seawater (i.e.,  $O_2 > 10 \mu M$ ) ca. 2.88–2.80 Ga. This is supported by the negative Ce anomalies in the Dianzihe iron formation (Fig. S4) that are indicative of oxic seawater, since oxidation and removal of Ce are closely associated with Mn (oxyhydr)oxides.

The Fe isotope composition of the Dianzihe iron formation adds further evidence for oxygenated seawater and its redox structure in the Mesoarchean oceans. Given the substantial Fe isotope fractionation (up to  $\sim 3\%$  in  $\delta^{56}Fe$ ) between precipitated Fe(III) oxyhydroxides and aqueous Fe(II) (Li et al., 2013), massive removal of high- $\delta^{56}Fe$  Fe(III) oxyhydroxides would leave significant low- $\delta^{56}Fe$  Fe(II) in seawater during iron formation deposition (Rouxel et al., 2005; Li et al., 2013). The  $\delta^{56}Fe$  values of the Dianzihe iron formation samples range from  $-0.21$  to  $-1.33\%$ , with an average of  $-0.91\%$  (Fig. 2). These  $\delta^{56}Fe$  values are comparable to the most  $\delta^{56}Fe$ -depleted and Mn-rich iron formations deposited shortly before or during the GOE (e.g., Kurzweil et al., 2016). We used a Rayleigh fractionation model (Fig. S8) to simulate the change in  $\delta^{56}Fe$  values of Fe oxyhydroxides and ambient seawater during deposition of the Dianzihe iron formation. The  $\delta^{56}Fe$  variation in the Dianzihe iron formation can best be explained by extensive oxidation of low- $\delta^{56}Fe$  Fe(II) in oxygenated seawater. For instance, assuming  $\delta^{56}Fe$  values of a primary Fe(II) pool are  $-2\%$  and  $-3\%$ , the oxidation of 61%–92% and 13%–65% the Fe(II), respectively, can account for the deposition of the Dianzihe iron formation.

The  $\delta^{56}Fe$  values of the Dianzihe iron formation are also positively correlated with Mn enrichment (i.e., Fe/Mn ratio) (Fig. 2). This correlation suggests that the iron formation was deposited in oxygenated seawater that may have a depth-related redox gradient (Fig. 3). Given the strong kinetic limitation of Mn(II) oxidation by  $O_2$  (Morgan, 2005) and the potential oxidation of Fe(II) by Mn(III)/Mn(IV), the preferential precipitation of high- $\delta^{56}Fe$  Fe(III) oxyhydroxides would have resulted in deposition of the iron formation samples with high Fe/Mn ratio, leading to a decrease in the  $\delta^{56}Fe$  values and Fe/Mn ratios in suboxic (e.g., 1–10  $\mu M O_2$ ) seawater. This Mn(II)- and low- $\delta^{56}Fe$  Fe(II)-bearing seawater, which may also have contained low- $\delta^{56}Fe$  Fe(II) produced by dissimilatory iron reduction, could have upwelled or advected into a shallower, oxic (e.g.,  $> 10 \mu M O_2$ ) environment. Consequently, the later-stage precipitation of Fe(III) oxyhydroxides and

- ◆ ca. 2.90 Ga IFs from the Sinqeni Formation (South Africa)
- ca. 2.88–2.80 Ga Dianzihe IF from the Kongling Complex (South China)
- ca. 2.46–2.40 Ga IFs from the Ghaap Group (South African)
- ▲ ca. 1.88 Ga IFs from the Laurasia
- Modern redox-stratified water column in Pavin lake (France)
- + Modern submarine hydrothermal vent fluids (North Pacific Ocean)

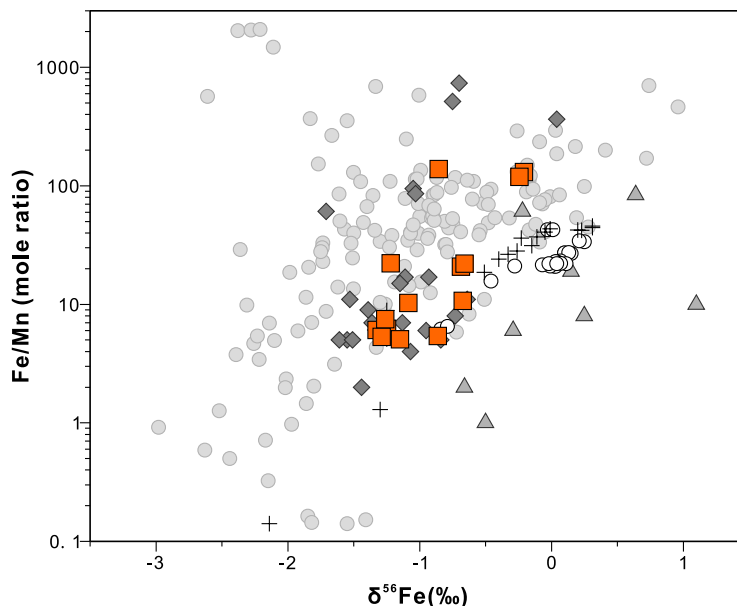


**Figure 2. The positive correlation between  $\delta^{56}Fe$  values and Fe/Mn ratios in iron formations (IFs) supports the existence of oxygenated seawater before, during, and after the Great Oxidation Event (see main text for details). Data sources are provided in Fig. S9 (see text footnote 1).**

MnOx in oxic seawater would have lighter Fe isotope compositions and lower Fe/Mn ratios (Busigny et al., 2014; Kurzweil et al., 2016; Huang et al., 2021). Therefore, the oxidation of Fe(II) and Mn(II) in suboxic–oxic seawater (e.g., 1 to  $> 10 \mu M O_2$ ) would naturally establish

a positive correlation between low  $\delta^{56}Fe$  values and Mn enrichment in iron formations.

The alternating laminations in the Dianzihe iron formation suggest that the iron formation was deposited below wave base (e.g., 30–50 m). This supports that the oxygenated seawater (i.e.,

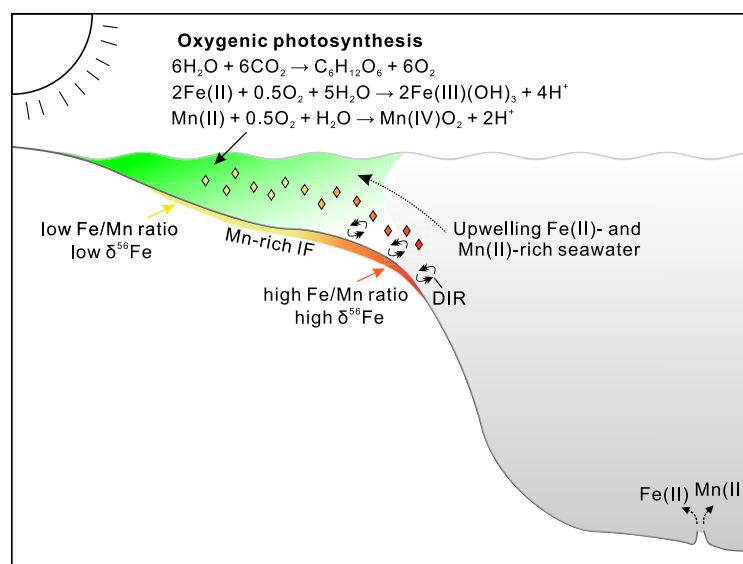


**Figure 3. A model for deposition of the Mn-rich Dianzihe iron formation in a Mesoarchean oxygen oasis. With the preferential precipitation of high- $\delta^{56}Fe$  Fe(III) oxyhydroxides, the oxygenated seawater gradually evolved toward lighter Fe isotope compositions and lower Fe/Mn ratios. Microbial dissimilatory iron reduction (DIR) may have produced another source of low- $\delta^{56}Fe$  Fe(II). The oxidation of upwelling Mn(II) and low- $\delta^{56}Fe$  Fe(II) eventually formed the Mn-rich iron formation in oxic (i.e.,  $> 10 \mu M O_2$ ) seawater.**

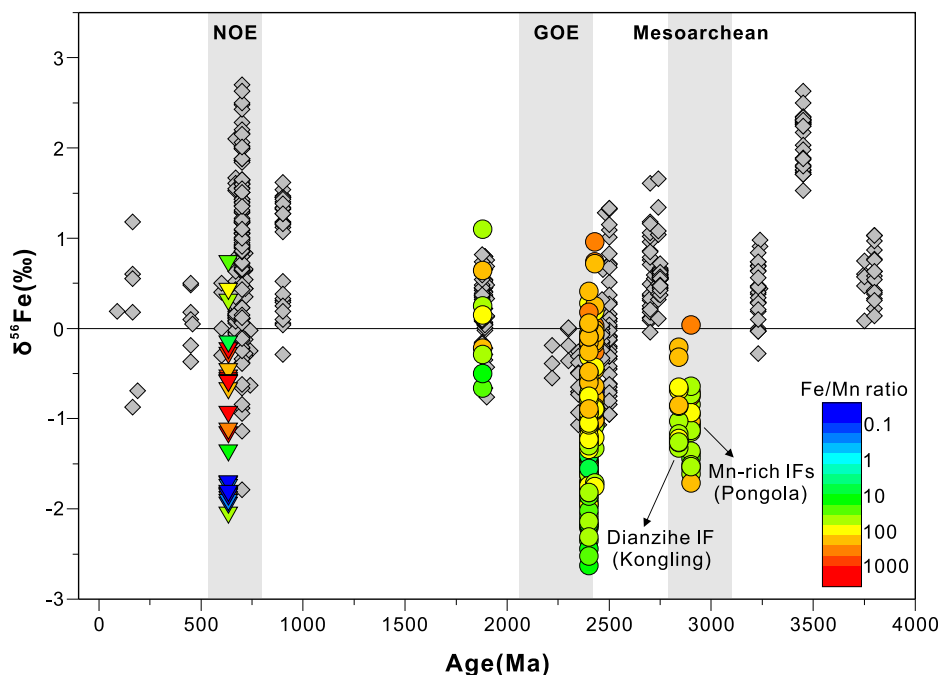


**Figure 4. Temporal distribution of low- $\delta^{56}\text{Fe}$  Mn-rich iron formations (IF) is closely associated with oxygenation events over geological time (modified after Huang et al., 2021). Dark gray diamonds—Fe-oxide-bearing chemical sediments (mostly iron formations); colored circles and triangles—Mn-rich iron formations deposited during the Archean to Neoproterozoic; GOE—Great Oxidation Event; NOE—Neoproterozoic Oxygenation Event.**

1 to  $>10 \mu\text{M O}_2$ ) from which the iron formation deposited likely existed in localized shallow marine environments (e.g., nearshore) in the Mesoarchean oceans, which is consistent with previous estimates of 1 to a few tens of  $\mu\text{M O}_2$  in the Archean oxygen oases (Czaja et al., 2012; Olson et al., 2013; Ossa Ossa et al., 2018). Given that temporal distribution of low- $\delta^{56}\text{Fe}$  Mn-rich iron formations was closely associated with oxygenation events throughout the Precambrian (Huang et al., 2021) (Fig. 4), the regional-scale oxygenated seawater from which Mn-rich iron formations deposited was unlikely to have resulted from non-photosynthetic mechanisms, indicative of cyanobacterial  $\text{O}_2$  production at that time.

## CONCLUSIONS AND IMPLICATIONS

Combined geochronological, multiple-scale petrographic, major trace element, and Fe isotope analyses of the Mesoarchean Mn-rich Dianzihe iron formation in South China reveal the precipitation of  $\text{MnO}_x$ , simultaneous Mn enrichment, and a low- $\delta^{56}\text{Fe}$  signal during deposition of this iron formation. Our findings provide compelling evidence for cyanobacterial  $\text{O}_2$  production at that time. The observed correlation between  $\delta^{56}\text{Fe}$  values and Mn enrichment in iron formations is linked to  $\text{O}_2$  level, possibly reflecting a depth-related redox gradient where  $\text{O}_2$  concentrations varied from a few to  $>10 \mu\text{M}$ .

The earliest known Mn-rich iron formations, found in the Pongola Supergroup and Kongling Complex (Fig. 4), date back to the Mesoarchean,

supporting the notion that oxygenic photosynthesis was already established at that time (e.g., Crowe et al., 2013; Planavsky et al., 2014; Ossa Ossa et al., 2018). More importantly, the two locations underwent distinct geological histories ca. 3.0–2.8 Ga (Guo et al., 2015; Luskin et al., 2019), suggesting that the two Mn-rich iron formations occupied different paleogeographic locations during the Mesoarchean. The significance of this is that the oxygen oases, driven by cyanobacterial  $\text{O}_2$  production, may have already been globally distributed in Mesoarchean oceans.

## ACKNOWLEDGMENTS

We are grateful to Kathleen C. Benison for editorial handling, Matthew Brzozowski for insightful discussions, and Frantz-Gerard Ossa Ossa as well as an anonymous reviewer for their constructive comments and suggestions that greatly improved the manuscript. We thank Kai Gan and Ben Dang for their assistance during the field sampling and Dehong Du for his assistance with Fe isotope analyses. This study was financially supported by the Xinjiang Key Research and Development Program (2024B03004), the National Natural Science Foundation of China (42203068, 41872077, 42425301), and the Tianchi Talents Introduction Plan of Xinjiang to Wu.

## REFERENCES CITED

- Brocks, J.J., 2011, Millimeter-scale concentration gradients of hydrocarbons in Archean shales: Live-oil escape or fingerprint of contamination? *Geochimica et Cosmochimica Acta*, v. 75, p. 3196–3213, <https://doi.org/10.1016/j.gca.2011.03.014>.
- Busigny, V., Planavsky, N.J., Jézéquel, D., Crowe, S., Louvat, P., Moureau, J., Viollier, E., and Lyons,

- T.W., 2014, Iron isotopes in an Archean ocean analogue: *Geochimica et Cosmochimica Acta*, v. 133, p. 443–462, <https://doi.org/10.1016/j.gca.2014.03.004>.
- Cardona, T., 2017, Photosystem II is a chimera of reaction centers: *Journal of Molecular Evolution*, v. 84, p. 149–151, <https://doi.org/10.1007/s00239-017-9784-x>.
- Crowe, S.A., Døssing, L.N., Beukes, N.J., Bau, M., Kruger, S.J., Frei, R., and Canfield, D.E., 2013, Atmospheric oxygenation three billion years ago: *Nature*, v. 501, p. 535–538, <https://doi.org/10.1038/nature12426>.
- Czaja, A.D., Johnson, C.M., Roden, E.E., Beard, B.L., Voegelin, A.R., Nägler, T.F., Beukes, N.J., and Wille, M., 2012, Evidence for free oxygen in the Neoproterozoic ocean based on coupled iron–molybdenum isotope fractionation: *Geochimica et Cosmochimica Acta*, v. 86, p. 118–137, <https://doi.org/10.1016/j.gca.2012.03.007>.
- Daye, M., Klepac-Ceraj, V., Pajusalu, M., Rowland, S., Farrell-Sherman, A., Beukes, N., Tamura, N., Fournier, G., and Bosak, T., 2019, Light-driven anaerobic microbial oxidation of manganese: *Nature*, v. 576, p. 311–314, <https://doi.org/10.1038/s41586-019-1804-0>.
- Eickmann, B., Hofmann, A., Wille, M., Bui, T.H., Wing, B.A., and Schoenberg, R., 2018, Isotopic evidence for oxygenated Mesoarchean shallow oceans: *Nature Geoscience*, v. 11, p. 133–138, <https://doi.org/10.1038/s41561-017-0036-x>.
- Gao, S., Ling, W., Qiu, Y., Lian, Z., Hartmann, G., and Simon, K., 1999, Contrasting geochemical and Sm–Nd isotopic compositions of Archean metasediments from the Kongling high-grade terrain of the Yangtze craton: Evidence for cratonic evolution and redistribution of REE during crustal anatexis: *Geochimica et Cosmochimica Acta*, v. 63, p. 2071–2088, [https://doi.org/10.1016/S0016-7037\(99\)00153-2](https://doi.org/10.1016/S0016-7037(99)00153-2).
- Guo, J.-L., Wu, Y.-B., Gao, S., Jin, Z.-M., Zong, K.-Q., Hu, Z.-C., Chen, K., Chen, H.-H., and Liu, Y.-S., 2015, Episodic Paleoproterozoic–Neoproterozoic (3.3–2.0 Ga) granitoid magmatism in Yangtze Craton, South China: Implications for late Archean tectonics: *Precambrian Research*, v. 270, p. 246–266, <https://doi.org/10.1016/j.precamres.2015.09.007>.
- Herndon, E.M., Havig, J.R., Singer, D.M., McCormick, M.L., and Kump, L.R., 2018, Manganese and iron geochemistry in sediments underlying the redox-stratified Fayetteville Green Lake: *Geochimica et Cosmochimica Acta*, v. 231, p. 50–63, <https://doi.org/10.1016/j.gca.2018.04.013>.
- Huang, Q., Viehmann, S., Walde, D.H.G., and Li, W., 2021, Iron isotope constraints on the metal source and depositional environment of the Neoproterozoic banded iron- and manganese deposits in Urucum, Brazil: *Geochemistry*, v. 81, <https://doi.org/10.1016/j.chemer.2021.125771>.
- Johnson, J.E., Webb, S.M., Thomas, K., Ono, S., Kirschvink, J.L., and Fischer, W.W., 2013, Manganese-oxidizing photosynthesis before the rise of cyanobacteria: *Proceedings of the National Academy of Sciences of the United States of America*, v. 110, p. 11,238–11,243, <https://doi.org/10.1073/pnas.1305530110>.
- Johnson, K.S., Berelson, W.M., Coale, K.H., Coley, T.L., Elrod, V.A., Fairley, W.R., Iams, H.D., Kilgore, T.E., and Nowicki, J.L., 1992, Manganese flux from continental margin sediments in a transect through the oxygen minimum: *Science*, v. 257, p. 1242–1245, <https://doi.org/10.1126/science.257.5074.1242>.
- Klein, C., 2005, Some Precambrian banded iron-formations (BIFs) from around the world: Their age, geologic setting, mineralogy, metamorphism,

- geochemistry, and origins: *American Mineralogist*, v. 90, p. 1473–1499, <https://doi.org/10.2138/am.2005.1871>.
- Knoll, A.H., 2003, The geological consequences of evolution: *Geobiology*, v. 1, p. 3–14, <https://doi.org/10.1046/j.1472-4669.2003.00002.x>.
- Konhauser, K.O., et al., 2017, Iron formations: A global record of Neoproterozoic to Palaeoproterozoic environmental history: *Earth-Science Reviews*, v. 172, p. 140–177, <https://doi.org/10.1016/j.earscirev.2017.06.012>.
- Kurzweil, F., Wille, M., Gantert, N., Beukes, N.J., and Schoenberg, R., 2016, Manganese oxide shuttling in pre-GOE oceans—Evidence from molybdenum and iron isotopes: *Earth and Planetary Science Letters*, v. 452, p. 69–78, <https://doi.org/10.1016/j.epsl.2016.07.013>.
- Li, L., Lin, S., Davis, D.W., Xiao, W., Xing, G., and Yin, C., 2014, Geochronology and geochemistry of igneous rocks from the Kongling terrane: Implications for Mesoarchean to Paleoproterozoic crustal evolution of the Yangtze Block: *Precambrian Research*, v. 255, p. 30–47, <https://doi.org/10.1016/j.precamres.2014.09.009>.
- Li, W., Huberty, J.M., Beard, B.L., Kita, N.T., Valley, J.W., and Johnson, C.M., 2013, Contrasting behavior of oxygen and iron isotopes in banded iron formations revealed by in situ isotopic analysis: *Earth and Planetary Science Letters*, v. 384, p. 132–143, <https://doi.org/10.1016/j.epsl.2013.10.014>.
- Liu, W., Hao, J., Elzenga, E.J., Piotrowiak, P., Nanda, V., Yee, N., and Falkowski, P.G., 2020, Anoxic photogeochemical oxidation of manganese carbonate yields manganese oxide: *Proceedings of the National Academy of Sciences of the United States of America*, v. 117, p. 22,698–22,704, <https://doi.org/10.1073/pnas.2002175117>.
- Luskin, C., Wilson, A., Gold, D., and Hofmann, A., 2019, The Pongola Supergroup: Mesoarchean deposition following Kaapvaal Craton stabilization, in Kröner, A., and Hofmann, A., eds., *The Archaean Geology of the Kaapvaal Craton, Southern Africa*: Cham, Springer International Publishing, *Regional Geology Reviews*, p. 225–254, [https://doi.org/10.1007/978-3-319-78652-0\\_9](https://doi.org/10.1007/978-3-319-78652-0_9).
- Lyons, T.W., Diamond, C.W., and Konhauser, K.O., 2020, Shedding light on manganese cycling in the early oceans: *Proceedings of the National Academy of Sciences of the United States of America*, v. 117, p. 25,960–25,962, <https://doi.org/10.1073/pnas.2016447117>.
- Lyons, T.W., Reinhard, C.T., and Planavsky, N.J., 2014, The rise of oxygen in Earth's early ocean and atmosphere: *Nature*, v. 506, p. 307–315, <https://doi.org/10.1038/nature13068>.
- Morgan, J.J., 2005, Kinetics of reaction between O<sub>2</sub> and Mn(II) species in aqueous solutions: *Geochimica et Cosmochimica Acta*, v. 69, p. 35–48, <https://doi.org/10.1016/j.gca.2004.06.013>.
- Olson, S.L., Kump, L.R., and Kasting, J.F., 2013, Quantifying the areal extent and dissolved oxygen concentrations of Archean oxygen oases: *Chemical Geology*, v. 362, p. 35–43, <https://doi.org/10.1016/j.chemgeo.2013.08.012>.
- Ossa Ossa, F., Hofmann, A., Wille, M., Spangenberg, J.E., Bekker, A., Poulton, S.W., Eickmann, B., and Schoenberg, R., 2018, Aerobic iron and manganese cycling in a redox-stratified Mesoarchean epicontinental sea: *Earth and Planetary Science Letters*, v. 500, p. 28–40, <https://doi.org/10.1016/j.epsl.2018.07.044>.
- Ostrander, C.M., Johnson, A.C., and Anbar, A.D., 2021, Earth's First Redox Revolution: *Annual Review of Earth and Planetary Sciences*, v. 49, p. 337–366, <https://doi.org/10.1146/annurev-earth-072020-055249>.
- Planavsky, N.J., et al., 2014, Evidence for oxygenic photosynthesis half a billion years before the Great Oxidation Event: *Nature Geoscience*, v. 7, p. 283–286, <https://doi.org/10.1038/ngeo2122>.
- Poulton, S.W., Bekker, A., Cumming, V.M., Zerkle, A.L., Canfield, D.E., and Johnston, D.T., 2021, A 200-million-year delay in permanent atmospheric oxygenation: *Nature*, v. 592, p. 232–236, <https://doi.org/10.1038/s41586-021-03393-7>.
- Qiu, Y.M., Gao, S., McNaughton, N.J., Groves, D.I., and Ling, W., 2000, First evidence of >3.2 Ga continental crust in the Yangtze craton of south China and its implications for Archean crustal evolution and Phanerozoic tectonics: *Geology*, v. 28, p. 11–14, [https://doi.org/10.1130/0091-7613\(2000\)028<0011:FEOGCC>2.0.CO;2](https://doi.org/10.1130/0091-7613(2000)028<0011:FEOGCC>2.0.CO;2).
- Robbins, L.J., et al., 2023, Manganese oxides, Earth surface oxygenation, and the rise of oxygenic photosynthesis: *Earth-Science Reviews*, v. 239, <https://doi.org/10.1016/j.earscirev.2023.104368>.
- Rouxel, O.J., Bekker, A., and Edwards, K.J., 2005, Iron isotope constraints on the Archean and Paleoproterozoic ocean redox state: *Science*, v. 307, p. 1088–1091, <https://doi.org/10.1126/science.1105692>.
- Sánchez-Baracaldo, P., Bianchini, G., Wilson, J.D., and Knoll, A.H., 2022, Cyanobacteria and biogeochemical cycles through Earth history: *Trends in Microbiology*, v. 30, p. 143–157, <https://doi.org/10.1016/j.tim.2021.05.008>.
- Wittkop, C., Swanner, E.D., Grengs, A., Lambrecht, N., Fakhraee, M., Myrbo, A., Bray, A.W., Poulton, S.W., and Katsev, S., 2020, Evaluating a primary carbonate pathway for manganese enrichments in reducing environments: *Earth and Planetary Science Letters*, v. 538, <https://doi.org/10.1016/j.epsl.2020.116201>.
- Zhou, H., Zhou, W., Wei, Y., Chi Fru, E., Huang, B., Fu, D., Li, H., and Tan, M., 2022, Mesoarchean banded iron-formation from the northern Yangtze Craton, South China and its geological and paleoenvironmental implications: *Precambrian Research*, v. 383, <https://doi.org/10.1016/j.precamres.2022.106905>.

Printed in the USA